

# Two Co(II)-based Coordination Polymers Constructed from $\pi$ -electron-rich Polycarboxylate Aryl Ether Ligand: Structural Insights and Photocatalytic Dye Degradation

WANG Xiao-Feng<sup>a</sup> GUO Xin-Yu<sup>b</sup> LIU Tao<sup>a①</sup>

<sup>a</sup> (School of Hydraulic and Electric Power, Heilongjiang University, Harbin 150080, China)

<sup>b</sup> (College of Science, Northeast Agricultural University, Harbin 150038, China)

**ABSTRACT** In the present study, two new Co(II)-based coordination polymers (CPs) with chemical formulas of  $\{[\text{Co}_3(\mu_3\text{-OH})(\text{L})(\text{H}_2\text{O})_3] \cdot 2\text{H}_2\text{O}\}_n$  (**1**) and  $\{[\text{Co}_3(\mu_3\text{-OH})(\text{L})(\text{H}_2\text{O})] \cdot 2\text{DMF} \cdot 3\text{H}_2\text{O}\}_n$  (**2**) have been successfully prepared by the reaction of  $\text{Co}(\text{NO}_3)_2 \cdot 6\text{H}_2\text{O}$  with  $\pi$ -electron-rich polycarboxylate aryl ether ligand 5,5'-((5-carboxy-1,3-phenylene)bis(oxy))diisophthalic acid ( $\text{H}_5\text{L}$ ) under different solvothermal reaction conditions. Both CPs have been studied via single-crystal X-ray diffraction, powder X-ray diffraction (PXRD) and thermogravimetric analysis (TGA). The photophysical studies indicated that complex **2** with good water stability is a potential semiconductive material, which could be applied for the degradation of methylene blue (MB) under UV light irradiation and exhibit good stability and recyclability.

**Keywords:** coordination polymer, structural diversity, aryl ether ligand, dye degradation;

**DOI:** 10.14102/j.cnki.0254-5861.2011-3046

## 1 INTRODUCTION

Within the last decade, the researches on different metal-organic architectures including CPs (coordination polymers) have become an exceptionally important multidisciplinary field covering various branches of chemistry, materials science and beyond<sup>[1-4]</sup>. Such extraordinary attention to CPs is primarily driven by their enormous structural diversity, unique porosity and multifaceted functional properties that enable a vast variety of applications. Despite the enormous progress made in the design and synthesis of coordination polymers with target structures and properties, there are still many challenges concerning the reproducibility, scalability and sustainability of synthetic protocols for CPs<sup>[5-8]</sup>.

Many metal-organic architectures are prepared *via* self-assembly or solvo(hydro) thermal protocols, the efficiency and output of which can be affected by numerous factors, including the coordination preferences and nature of metal ions and organic building blocks, stoichiometry, solvent composition and other reaction parameters<sup>[9-11]</sup>. Among various types of linker ligands utilized for the construction of

CPs, aromatic polycarboxylic acids represent the most widely applied class of organic building blocks on account of their chemical and thermal stability, coordination versatility, and notable physicochemical properties. In this regard, polycarboxylic acids with an aromatic-ether functionality are particularly intriguing building blocks, which feature interesting flexibility and conformational diversity, and may enable the generation of uncommon or topologically unique metal-organic architectures<sup>[12-16]</sup>. In this work, we have chosen an ether-bridged tetracarboxylic acid, namely 5,5'-((5-carboxy-1,3-phenylene)bis(oxy))diisophthalic acid ( $\text{H}_5\text{L}$ ), and probed its application toward the generation of Co(II)-based coordination polymers. Two new Co(II)-based coordination polymers (CPs),  $\{[\text{Co}_3(\mu_3\text{-OH})(\text{L})(\text{H}_2\text{O})_3] \cdot 2\text{H}_2\text{O}\}_n$  (**1**) and  $\{[\text{Co}_3(\mu_3\text{-OH})(\text{L})(\text{H}_2\text{O})] \cdot 2\text{DMF} \cdot 3\text{H}_2\text{O}\}_n$  (**2**), have been successfully produced under different solvothermal reaction conditions. Both CPs have been studied via single-crystal X-ray diffraction, powder X-ray diffraction (PXRD) as well as thermogravimetric analysis (TGA). The photophysical studies indicated that complex **2** with good water stability is a potential semiconductive material, which could be applied for the degradation of

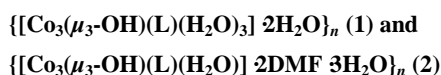
methylene blue (MB) under UV light irradiation and exhibit good stability and recyclability.

## 2 EXPERIMENTAL

### 2.1 Chemicals and measurements

All reagents were of analytical reagent grade and obtained from commercial suppliers. H<sub>5</sub>L was acquired from Jinan Henghua Sci. & Tech. Co., Ltd. A Bruker EQUINOX 55 spectrometer was used to record the FT-IR spectra (KBr discs). An Elementar Vario EL elemental analyzer was employed to perform the C/H/N elemental analyses (EA). A LINSEIS STA PT1600 thermal analyzer was used to perform the thermogravimetric analyses (TGA) under a N<sub>2</sub> flow at a heating rate of 10 °C min<sup>-1</sup>. A Rigaku-Dmax 2400 diffractometer (CuK $\alpha$  radiation,  $\lambda$  = 1.54060 Å) was used to obtain the powder X-ray diffraction patterns (PXRD). UV-vis DRS spectra were obtained by a Cary 300 UV-vis spectrophotometer (Agilent, USA) using BaSO<sub>4</sub> as the internal standard reference.

### 2.2 Preparation and characterization for



H<sub>5</sub>L (0.05 mmol, 24.1 mg) and Co(NO<sub>3</sub>)<sub>2</sub> · 6H<sub>2</sub>O (0.15 mmol, 45 mg) were dissolved in a solvent mixture of 3 mL diethylformamide (DEF) and 1 mL H<sub>2</sub>O. The solution was autoclaved at 110 °C for 3 days, and then slowly cooled to room temperature (r.t.), giving rise to rectangular block-shaped pink crystals in 46% yield (based on Co(II)). Elemental analysis (%) calcd. for C<sub>23</sub>H<sub>20</sub>O<sub>18</sub>Co<sub>3</sub> (1): C, 36.29; H, 2.65. Found (%): C, 36.43; H, 2.61. FT-IR (KBr, cm<sup>-1</sup>): 3426 (m), 1649 (s), 1568 (s), 1457 (m), 1391 (s), 1132 (w), 1016 (w), 777 (m), 726 (w), 671 (w).

The synthesis protocol of 2 was similar to that of 1, except that DEF in the mixed solvent was replaced with dimethylformamide (DMF). The block-shaped pink crystals were obtained in 46% yield (based on Co(II)). Elemental analysis (%) calcd. for C<sub>29</sub>H<sub>32</sub>O<sub>19</sub>N<sub>2</sub>Co<sub>3</sub>: C, 39.16; H, 3.63; N, 3.15. Found (%): C, 39.28; H, 3.57; N, 3.14. FT-IR (KBr, cm<sup>-1</sup>): 3368 (m), 1624 (s), 1573 (s), 1380 (s), 1249 (m), 1137 (m), 1016 (m), 782 (s), 726 (m), 665 (w).

### 2.3 Crystal structure determination

A green block-shaped single crystal of complex 1 (0.24 mm × 0.21 mm × 0.22 mm) and a blue block-shaped single crystal of complex 2 (0.23 mm × 0.20 mm × 0.20 mm) were placed on an APEX II CCD area detector equipped with a graphite-

monochromatic MoK $\alpha$  radiation ( $\lambda$  = 0.71073 Å) at 293(2) K. For complexes 1 and 2, a total of 34558 and 46091 reflections were collected, of which 6885 ( $R_{\text{int}}$  = 0.0436) and 6564 ( $R_{\text{int}}$  = 0.0850) were independent in the  $\varphi$ - $\omega$  ranges of 3.40~28.95 ° and 2.35~25.00 °, and 5524 and 5202 observed reflections with  $I > 2\sigma(I)$  were employed for structure refinements, respectively.

The empirical absorption corrections by SADABS were carried out. The structures were solved by direct methods with SHELXS-97 program and refined with SHELXL-97 by full-matrix least-squares techniques. The non-hydrogen atoms were refined anisotropically, and the hydrogen ones were determined with theoretical calculations<sup>[17]</sup>. For complex 1, the final  $R$  = 0.0374,  $wR$  = 0.0946 ( $w = 1/[\sigma^2(F_o^2) + (0.1000P)^2 + 0.0000P]$ , where  $P = (F_o^2 + 2F_c^2)/3$ ),  $(\Delta/\sigma)_{\text{max}}$  = 0.001,  $S$  = 1.011,  $(\Delta\rho)_{\text{max}}$  = 0.365 and  $(\Delta\rho)_{\text{min}}$  = -0.240 e/Å<sup>3</sup>. For complex 2, the final  $R$  = 0.0477,  $wR$  = 0.1312 ( $w = 1/[\sigma^2(F_o^2) + (0.1000P)^2 + 0.0000P]$ , where  $P = (F_o^2 + 2F_c^2)/3$ ),  $(\Delta/\sigma)_{\text{max}}$  = 0.000,  $S$  = 1.056,  $(\Delta\rho)_{\text{max}}$  = 1.586 and  $(\Delta\rho)_{\text{min}}$  = -1.021 e/Å<sup>3</sup>. Complex 1 crystallizes in orthorhombic, space group  $Pmn2_1$  with  $a$  = 17.4263(2),  $b$  = 11.7155(1),  $c$  = 13.9426(2) Å,  $V$  = 2846.49(6) Å<sup>3</sup>,  $Z$  = 2,  $F(000)$  = 746,  $D_c$  = 0.867 mg/m<sup>3</sup> and  $\mu$  = 0.903 mm<sup>-1</sup>. Complex 2 crystallizes in triclinic, space group  $P\bar{1}$  with  $a$  = 10.1200(5),  $b$  = 12.3807(6),  $c$  = 15.6793(8) Å,  $V$  = 1870.59(16) Å<sup>3</sup>,  $Z$  = 2,  $F(000)$  = 868,  $D_c$  = 1.223 Mg/m<sup>3</sup> and  $\mu$  = 1.364 mm<sup>-1</sup>.

## 3 RESULTS AND DISCUSSION

### 3.1 Crystal structures

Single-crystal X-ray analysis revealed that complex 1 crystallizes in orthorhombic system, space group  $Pmn2_1$ . Each asymmetric unit consists of one and a half crystallographically independent Co(II) atoms, half of an L<sup>5-</sup> ligand, one  $\mu_3$ -OH, and two and a half water molecules. Co(1) is coordinated by three carboxylic oxygen atoms from three different L<sup>5-</sup> ligands and one  $\mu_3$ -OH oxygen atom. The structure displays a slightly distorted tetrahedral coordination geometry. Co(2) forms a distorted/twisted octahedral geometry with two oxygen atoms from two different L<sup>5-</sup> ligands, one  $\mu_3$ -OH oxygen atom and three oxygen atoms from three different lattice water molecules (Fig. 1a). Additionally, Co(1), Co(2), and Co(1A) share the  $\mu_3$ -OH oxygen atom to form trinuclear nodes [Co<sub>3</sub>( $\mu_3$ -OH)(H<sub>2</sub>O)<sub>3</sub>(COO)<sub>5</sub>], wherein the Co-O bond distances range from 1.94 to 2.19 Å. The fully deprotonated carboxylic

groups of the  $L^{5-}$  ligand link the Co(1) atoms via  $\mu_2\text{-}\eta^1\text{:}\eta^1$  and  $\mu_1\text{-}\eta^1\text{:}\eta^1$  bridging modes to form 1D infinite chains (Fig. 1b). Subsequently, these 1D chains are linked to each other to generate 2D layers, which in turn are further fused by Co(1), Co(2), and  $H_3L$  ligands into a 3D structure. As calculated by the PLATON program, the solvent-accessible void volume of **1** is 64.5%. This 3D framework comprises large honeycomb cavities ( $10.99\text{\AA} \times 13.13\text{\AA}$ ), and the  $\pi$ -electron-rich benzene rings and Lewis basic carboxylate moieties of the ligands are evenly distributed in the inner walls of the pore (Fig. 1c). To gain a better understanding of the framework, both the trinuclear nodes and  $L^{5-}$  ligands are simplified as 4-connected nodes, so that the structure of **1** could be regarded as a uninodal net with a topological point symbol of  $(6^6)$  (Fig. 1d).

Single-crystal X-ray diffraction analysis revealed that complex **2** crystallizes in triclinic system with  $P\bar{1}$  space group. Each asymmetric unit consists of three crystallographically unique Co(ii) atoms, one fully deprotonated  $L^{5-}$  ligand, one  $\mu_3\text{-OH}$ , one coordinated water molecule, two DMF molecules, and three lattice water molecules (squeezed by PLATON). The Co(1) atom is coordinated by three oxygen atoms from three different  $L^{5-}$  ligands, one  $\mu_3\text{-OH}$  group, and one  $\mu_2\text{-O}$  from a water

molecule (Fig. 2a). The Co(3) atom is coordinated by two oxygen atoms from two different ligands, one oxygen atom from the  $\mu_3\text{-OH}$  group and one  $\mu_2\text{-O}$  from a water molecule. The Co(2) atom is coordinated by three oxygen atoms from three different ligands and one oxygen atom from the  $\mu_3\text{-OH}$  group. The separations of Co–O bonds vary from 1.90 to 2.51  $\text{\AA}$ . Meanwhile, the Co(ii) atoms share the  $\mu_3\text{-OH}$  oxygen atoms and  $\mu_2\text{-H}_2\text{O}$  molecules to form hexanuclear nodes  $[\text{Co}_6(\mu_3\text{-OH})_2(\mu_2\text{-OH})_2(\text{COO})_{10}]$ , in which the distances of Co(1)⋯Co(2), Co(1)⋯Co(3), and Co(2)⋯Co(3) are 3.19, 3.43 and 3.48  $\text{\AA}$ , respectively (Fig. 2b). The carboxylic groups of the fully deprotonated  $L^{5-}$  ligand followed the  $\mu_2\text{-}\eta^1\text{:}\eta^1$  and  $\mu_1\text{-}\eta^1\text{:}\eta^1$  bridging modes. The Co(1) and Co(3) atoms linked the  $L^{5-}$  ligands to form 1D double chains along the *b* direction. Such chains are in turn connected by Co(2) atoms to give rise to 2D layers which are further interconnected into a 3D structure featuring a six-nuclear Co cluster node (Fig. 2c). The void space of the unit cell of **2** calculated by PLATON, after removing the guest solvent molecules, was found to be 45.3%. From the perspective of topology, the structure of **2** could be simplified as a 2-nodal net with a point symbol of  $(4^{10})_2(4^{28}6^{16}8)$ , wherein the hexanuclear clusters could be rationalized as a 10-connected node and the  $L^{5-}$  ligands as a 5-connected linker (Fig. 2d).

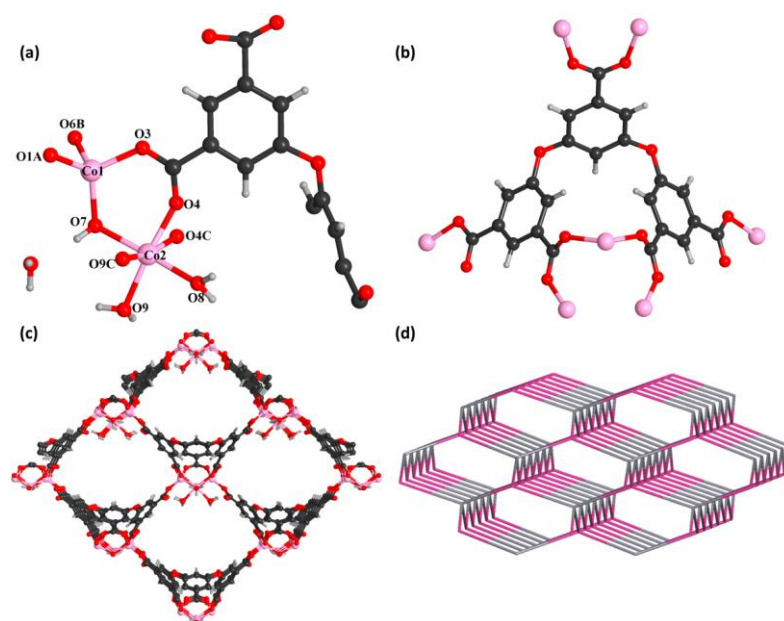


Fig. 1. (a) View for the asymmetry unit of **1** (symmetry codes A:  $1/2-x, -y, 1/2+z$ ; B:  $x, -1+y, z$ ; C:  $1-x, y, z$ ). (b) Coordination pattern for the  $L^{5-}$  ligand. (c) 3D network showing the 1D channels. (d) (4)-connected framework of **1**

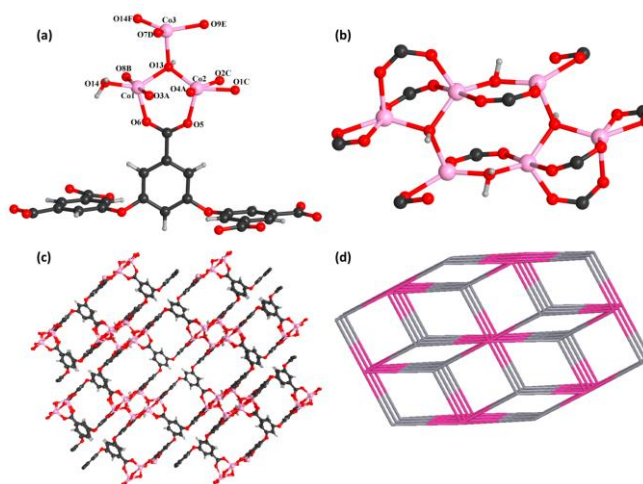


Fig. 2. (a) View for the asymmetry unit of **2** (symmetry codes A:  $1-x, 1-y, -z$ ; B:  $1-x, -y, 1-z$ ; C:  $-x, 1-y, -z$ ; D:  $x, 1+y, z$ ; E:  $-1+x, 1+y, z$ ; F:  $1-x, 1-y, 1-z$ ). (b) Co6 cluster of **2**. (c) 3D diagram of **2**. (d) (5,10)-connected network of **2**

### 3.2 PXRD and TGA

To check the phase purity of the products, powder X-ray diffraction (PXRD) experiments have been carried out for these complexes (Fig. 3). The peak positions of the experimental and simulated PXRD patterns are in good agreement with each other, indicating that the crystal structures are truly representative of the bulk crystal products. The differences in intensity may be owing to the preferred orientation of the crystal samples. Considering the following photocatalytic dye degradation experiments, it is necessary to study their framework stability in water. With this in mind, about 80 mg of the as-prepared crystalline samples of **1** and **2** were soaked in water for one day, and then the corresponding PXRD patterns were collected. As shown in Fig. 3a, no sharp peaks could be observed in the PXRD profiles, which indicates the framework of **1** collapses after water treatment. In comparison, the PXRD profile of **2** after water treatment shows a good match with those of the freshly as-prepared

ones, implying its good water stability. Such a difference of complexes **1** and **2** on the water stability might be related to their different cluster-based units and different connection. According to the previous literature, coordination polymers with high nuclear cluster and high connected nets usually show better water stability. Thermal stabilities of coordination polymers **1** and **2** were determined in the temperature range of  $20\sim 800\text{ }^{\circ}\text{C}$ . Complex **1** exhibits an initial weight loss of 11.8% (calcd. 11.5%) below  $160\text{ }^{\circ}\text{C}$  attributed to the release of water molecules. Subsequently, the TGA curve decreases slowly from  $186\text{ }^{\circ}\text{C}$  due to the degradation of the framework. Complex **2** displayed a primary weight loss of 23.4% (calcd. 24.0%) from r.t. to  $320\text{ }^{\circ}\text{C}$ , which denoted the removal of three water molecules and two DMF molecules squeezed by the SQUEEZE routine in PLATON. Subsequently, the entire framework began to degrade.

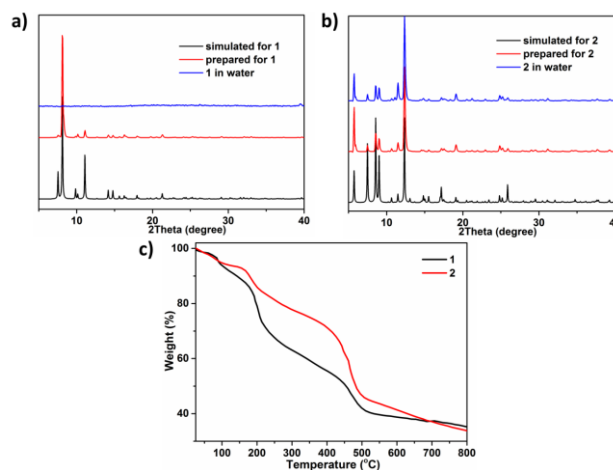


Fig. 3. (a) PXRD patterns of complex **1**; (b) PXRD patterns of complex **2**; (c) TGA curve of complexes **1** and **2**

### 3.3 Photocatalytic degradation experiments

In order to elucidate the photoresponse region, the solid state UV-vis diffuse reflection (DRS) spectra of complex **2** and the free organic ligand were measured at room temperature (Fig. 4a). The maximum UV absorption bands for the  $H_5L$  ligand are at *ca.* 254 and 296 nm, which may be attributed to the  $\pi \rightarrow \pi^*$  transition. Two absorption components in both UV and visible regions for complex **2** were observed. The UV absorption band (*ca.* 275 nm) can be attributed to the ligand-to-metal charge transfer (LMCT),

while the visible absorption band (*ca.* 548 nm) may be due to the  $d-d$  transition of the  $Co^{2+}$  ions. In previous investigations, the band gap energy ( $E_g$ ) was one of the key factors evaluating the degradation efficiency of the photocatalysts. Thus, the Kubelka-Munk (K-M) equation,  $F = (1 - R)^2/2R$ , where  $R$  is the reflectance of an infinitely thick layer at a given wavelength, was used to calculate the band gap energy ( $E_g$ ). The  $E_g$  value of **2** was estimated to be 2.78 eV (Fig. 4b), suggesting it may be responsive to UV light and has potential for photocatalytic reactions.

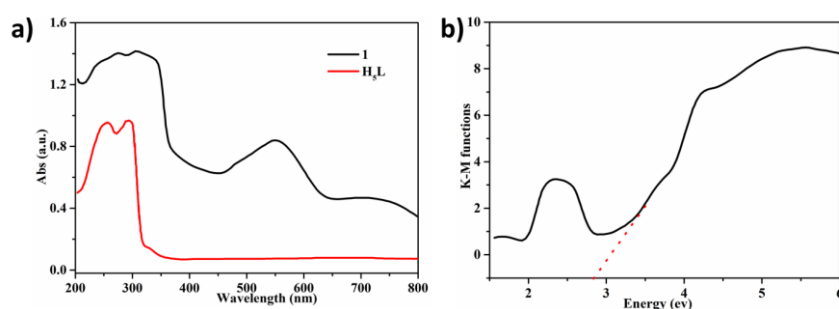


Fig. 4. (a) UV-vis absorption spectra of **2** and the free ligand in solid state; (b) Diffuse reflectance spectra of Kubelka-Munk functions *versus* energy (eV) for **2**

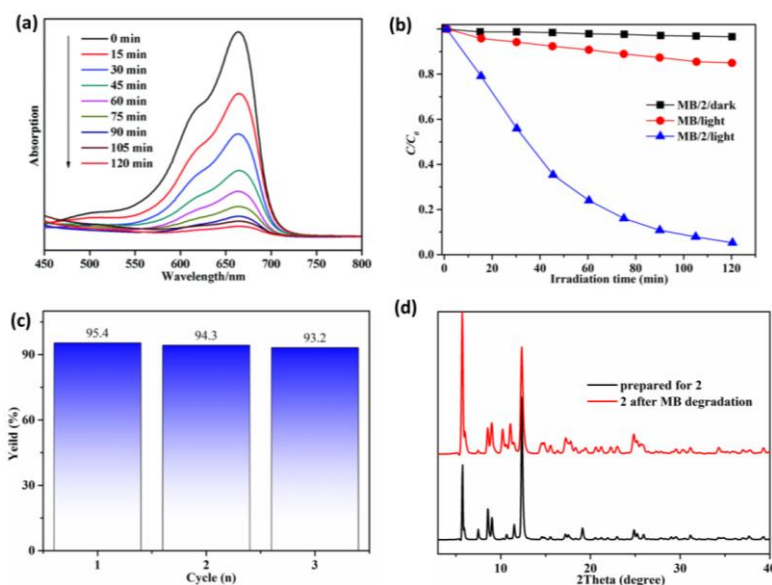


Fig. 5. (a) Absorption spectra of the MB solution during the decomposition reaction under UV irradiation with the presence of complex **2**. (b) Control experiments for photocatalytic degradation of the MB solution. (c) Cycling runs of **2** in the degradation of the MB solution. (d) PXRD patterns for **2** after dye degradation

As a chemically stable and poorly biodegradable dye, methylene blue (MB) is selected as a model dye contaminant to examine the photocatalytic activities of complex **2**. The characteristic absorption of MB at approximately 664 nm was used to monitor the process of photodegradation. It can be clearly seen that the absorption peaks of MB decreased

obviously with increasing the reaction time for **2** (Fig. 5a). The control experiment was also accomplished in the following reaction conditions: (1) in the dark; and (2) without any photocatalyst. When complex **2** was placed into an aqueous solution of MB in a dark environment for 120 min, there is no obvious decrease in the absorbance value, which

may avoid the possibility of adsorbing such a dye molecule into the frameworks and the catalytic degradation efficiency of MB is only 2.66% for **2**. In addition, the MB in the control experiment without any photocatalyst showed no noteworthy decrease in the absorbance value. The changes in the  $C_t/C_0$  plot of the MB solution against irradiation time are depicted in Fig. 5b, wherein  $C_0$  is the initial concentration of the MB solution and  $C_t$  is the concentration of the MB at any given time  $t$ . The calculations show that the photocatalytic efficiency increases from 11.9% (without any catalyst) to 94.5% for complex **2** after 120 min of UV irradiation. The increased photocatalytic degradation efficiency indicates that **2** is an excellent candidate as a photocatalyst in decomposing MB under UV light irradiation. The photocatalytic experiment was repeated to evaluate the reproducibility when using complex **2**. The photocatalytic performance of **2** in the repeated experiment did not significantly change after three cycles, indicating that the crystal materials were stable and

the experiments are reproducible for the photodegradation of MB under UV light irradiation (Fig. 5c). In addition, the PXRD measurements also confirm that the framework of **2** could keep its integrality in dye degradation process (Fig. 5d).

#### 4 CONCLUSION

In summary, we have successfully prepared two new Co-based coordination polymers *via* using the  $\pi$ -electron-rich polycarboxylate aryl ether ligand 5,5'-((5-carboxy-1,3-phenylene)bis(oxy))diisophthalic acid under different solvothermal reaction conditions. Due to their different cluster-based units and connection nets, they show different framework stability in water. Furthermore, complex **2** with better water stability is a potential semiconductive material, which could be applied for the degradation of methylene blue (MB) under UV light irradiation and exhibit good stability and recyclability.

#### REFERENCES

- (1) Wen, R. M.; Han, S. D.; Wang, H.; Zhang, Y. H. Synthesis, structure and magnetic properties of manganese(II) coordination polymer with azido and zwitterionic dicarboxylate ligand. *Chin. Chem. Lett.* **2014**, 25, 854–858.
- (2) Zhou, W.; Huang, D.; Wu, Y.; Zhao, J.; Wu, T.; Zhang, J.; Li, D.; Sun, C.; Feng, P.; Bu, X. Stable hierarchical bimetal-organic nanostructures as high performance electrocatalysts for the oxygen evolution reaction. *Angew. Chemie Int. Ed.* **2019**, 58, 4227–4231.
- (3) Huang, D.; Wu, X.; Tian, J.; Wang, X.; Zhou, Z.; Li, D. Assembling of a novel 3D Ag(I)-MOFs with mixed ligands tactics: syntheses, crystal structure and catalytic degradation of nitrophenol. *Chin. Chem. Lett.* **2018**, 29, 845–848.
- (4) Wei, J.; Yi, J.; Han, M.; Li, B.; Liu, S.; Wu, Y.; Ma, L.; Li, D. A water-stable terbium(III)-organic framework as a chemosensor for inorganic ions, nitro-containing compounds and antibiotics in aqueous solutions. *Chem. - An Asian J.* **2019**, 14, 3694–3701.
- (5) Wang, K.; Ma, X.; Shao, D.; Geng, Z.; Zhang, Z.; Wang, Z. Coordination-induced assembly of coordination polymer submicrospheres: promising antibacterial and in vitro anticancer activities. *Cryst. Growth Des.* **2012**, 12, 3786–3791.
- (6) Liu, J. J.; Xia, S. B.; Duan, Y. L.; Liu, T.; Cheng, F. X.; Sun, C. K. Anion-controlled architecture and photochromism of naphthalene diimide-based coordination polymers. *Polymers (Basel)* **2018**, 10, 165.
- (7) Xiao, Q. Q.; Liu, D.; Li, Y. H.; Cui, G. H. A 1D Co(II) coordination polymer based on semi-rigid bis(thiabendazole) and butane-1,2,3,4-tetracarboxylic acid linkers: synthesis, crystal structure, fluorescence sensing and photocatalytic properties. *Polyhedron* **2019**, 166, 65–72.
- (8) Wang, Y. N.; Wang, S. D.; Gao, Y. M.; Yang, L. L.; Xie, L. X. 3D Cadmium(II)-based coordination polymer constructed from V-shaped semirigid ligand: selective detection of oxoanion pollutants  $\text{CrO}_4^{2-}$ ,  $\text{Cr}_2\text{O}_7^{2-}$ ,  $\text{MnO}_4^-$  in water. *Zeitschrift Für Anorg. Und Allg. Chemie.* **2019**, 645, 1358–1364.
- (9) D'Vries, R. F.; De La Pena-O'Shea, V. A.; Benito Hernández, Á.; Snejko, N.; Gutiérrez-Puebla, E.; Monge, M. A. Enhancing metal-organic framework net robustness by successive linker coordination increase: from a hydrogen-bonded two-dimensional supramolecular net to a covalent one keeping the topology. *Cryst. Growth Des.* **2014**, 14, 5227–5233.
- (10) Sui, Q.; Yuan, Y.; Yang, N. N.; Li, X.; Gong, T.; Gao, E. Q.; Wang, L. Coordination-modulated piezochromism in metal-viologen materials. *J. Mater. Chem. C* **2017**, 5, 12400–12408.
- (11) Dutta, B.; Hazra, A.; Dey, A.; Sinha, C.; Ray, P. P.; Banerjee, P.; Mir, M. H. Construction of a succinate-bridged Cd(II)-based two-dimensional coordination polymer for efficient optoelectronic device fabrication and explosive sensing application. *Cryst. Growth Des.* **2020**, 20, 765–776.
- (12) Zhang, H. M.; He, Y. C.; Yang, J.; Liu, Y. Y.; Ma, J. F. Ten Coordination polymers constructed using an unprecedented azamacrocyclic octacarboxylate ligand 1,4,8,11-tetrazacyclododecane-N,N',N'',N'''-tetra-methylene-isophthalic acid: syntheses, structures, and photoluminescent

- properties. *Cryst. Growth Des.* **2014**, 14, 2307–2317.
- (13) Liang, X.; Jia, Y.; Zhan, Z.; Hu, M. A highly selective multifunctional Zn-coordination polymer sensor for detection of Cr(III), Cr(VI) ion, and TNP molecule. *Appl. Organomet. Chem.* **2019**, 33, 15399–15402.
- (14) Zou, G. D.; Huo, X. X.; Yu, X. C.; Tang, L.; Zhang, B.; Huang, X. Y. Three transition metal cluster-based coordination polymers based on 1,4-naphthalenedicarboxylate and pyridine ligands. *Inorg. Chem. Commun.* **2016**, 74, 16–21.
- (15) Haldar, R.; Matsuda, R.; Kitagawa, S.; George, S. J.; Maji, T. K. Amine-responsive adaptable nanospaces: fluorescent porous coordination polymer for molecular recognition. *Angew. Chemie - Int. Ed.* **2014**, 53, 11772–11777.
- (16) Hou, Y. F.; Liu, B.; Yue, K. F.; Zhou, C. S.; Wang, Y. M.; Yan, N.; Wang, Y. Y. Five solvent-induced cadmium coordination polymers (CPs) based on the same mixed ligands. *CrystEngComm.* **2014**, 16, 9560–9567.
- (17) Sheldrick, G. M. Crystal structure refinement with SHELXL. *Acta Crystallogr. Sect. C Struct. Chem.* **2015**, 71, 3–8.